Nanomedicine: Nanotechnology, Biology, and Medicine
34 (2021) 102377

nanomedicine
Nanotechnology, Biology, and Medicine

nanomedjournal.com

Low nanogel stiffness favors nanogel transcytosis across an in vitro blood–brain barrier

Laís Ribovski, PhD[a,b], Edwin de Jong, PhD[a], Olga Mergel, PhD[a], Guangyue Zu, MSc[a], Damla Keskin, MSc[a], Patrick van Rijn, PhD[a], Inge S. Zuhorn, PhD[a,*]

[a]*University of Groningen, University Medical Center Groningen, Department of Biomedical Engineering, Groningen, The Netherlands*
[b]*University of São Paulo, Physics Institute of São Carlos, Nanomedicine and Nanotoxicology Group, São Carlos, SP, Brazil*

Revised 23 December 2020

Abstract

Transport of therapeutics across the blood–brain barrier (BBB) is a fundamental requirement for effective treatment of numerous brain diseases. However, most therapeutics (>500 Da) are unable to permeate through the BBB and do not achieve therapeutic doses. Nanoparticles (NPs) are being investigated to facilitate drug delivery to the brain. Here, we investigate the effect of nanoparticle stiffness on NP transport across an *in vitro* BBB model. To this end, fluorescently labeled poly(*N*-isopropylmethacrylamide) (p(NIPMAM)) nanogels' stiffness was varied by the inclusion of 1.5 mol% (NG1.5), 5 mol% (NG5), and 14 mol% (NG14) *N*,*N*′-methylenebis(acrylamide) (BIS) cross-linker and nanogel uptake and transcytosis was quantified. The more densely cross-linked p(NIPMAM) nanogels showed the highest level of uptake by polarized brain endothelial cells, whereas the less densely cross-linked nanogels demonstrated the highest transcytotic potential. These findings suggest that nanogel stiffness has opposing effects on nanogel uptake and transcytosis at the BBB.

Key words: Nanoparticles; Blood–brain barrier; Nanogel; Stiffness; Transcytosis

Treatment and diagnosis of brain diseases, e.g., neurodegenerative diseases and brain cancer, are hindered by biological barriers, especially the blood–brain barrier (BBB). The BBB prevents compounds from reaching therapeutic concentrations in the brain, thereby hampering treatment efficacy and increasing side-effects and drug-resistance development. Nanoscale materials offer an opportunity to enhance treatment delivery, while materials' properties critically determine delivery efficacy. Nanoparticle (NP) characteristics, including size,[1–4] surface chemistry[2,5,6] as well as surface functionalization with target-specific ligands,[1,5,7–11] have been shown to influence NP transport across the BBB. One approach that is often used to enhance the transport of NPs across the BBB is to promote their endocytic uptake by brain endothelial cells.[8,9,12] However, in addition to NP uptake, the transcellular transport of NPs is also dependent on their intracellular trafficking and exocytosis. Yu et al[13] showed that high-affinity antibodies for the transferrin receptor accumulate to a lesser extent in the brain than low-affinity antibodies, because of enhanced trafficking to degradative lysosomes. Likewise, Wiley et al[14] coupled different amounts of transferrin (Tf) to gold nanoparticles and investigated their interaction with brain endothelial cells. They demonstrated that NPs with larger quantities of Tf bind to the BBB but do not accumulate in the brain parenchyma as efficiently as NPs with lower amounts of Tf, because of their inability to detach from the Tf-receptor at the basal side of the BBB. Understanding both how nanosized materials are transported into cells and how they get through cell barriers is essential to design drug delivery strategies.

It has been shown that hydrophilic rigid NPs show a higher uptake by macrophages, cancer, and endothelial cells than soft NPs at *in vitro* conditions.[15–22] Also, soft particles favor *in vivo* circulation, which leads to enhanced targeting at tumor sites, although the difference between soft and hard particles in blood persistence and tumor accumulation of the NPs seems more pronounced for short observation times.[15,16,18,23] Yi et al[24] suggested that, whereas rigid particles induce plasma membrane deformation, for a soft particle the membrane has no initial deformation but still needs to reach full enwrapping for its endocytosis, which therefore requires a higher adhesion energy. Although considerable efforts have been made to understand the

* Corresponding author.
E-mail address: i.zuhorn@umcg.nl (I.S. Zuhorn).

https://doi.org/10.1016/j.nano.2021.102377

cellular response to NP stiffness, both theoretically and experimentally, the effect of NP stiffness on its capacity to cross barrier cell types, including the BBB, is largely unexplored.

Nanogels (NGs) are nanoparticles composed of a cross-linked hydrophilic polymer network. Important aspects of NGs are their customizable stiffness and low level of protein adhesion.[25,26] NG stiffness can be easily modulated by varying the extent of polymer cross-linking, with minimal alterations to the NG composition. This offers an excellent opportunity to evaluate the influence of nanoparticle stiffness on fundamental biological cellular processes, including transcellular transport. Here, we explored the effect of the stiffness of p(NIPMAM) nanogels on their interaction with an *in vitro* BBB model. NGs of ~200 nm with varying stiffness were made by inclusion of 1.5 mol%, 5 mol%, and 14 mol% N,*N*′-methylenebis (acrylamide) (BIS) cross-linker during synthesis. The stiffer NG14 nanogel showed higher uptake by brain endothelial cells than the softer NG1.5 and NG5 nanogels. In contrast, NG1.5 and NG5 exhibited higher levels of transcytosis compared to NG14. An increase in the size of NG particles to ~400 nm, while keeping stiffness constant, was shown not to influence uptake or transcytosis. Altogether, our data suggest that nanogel stiffness has opposing effects on nanogel uptake and transcytosis at the BBB and that stiffness is a more determinant factor than size for the transcytosis of NG particles. Whereas high stiffness of NGs promotes uptake by brain endothelial cells, low NG stiffness stimulates transcytosis across the *in vitro* BBB.

Methods

Materials

N-isopropylmethacrylamide (97%, NIPMAM, #423548), *N*,*N*′ methylenebis(acrylamide) (99%, BIS, #146072), ammonium persulfate (98%, APS, #A3679), sodium dodecyl sulfate (SDS), ascorbic acid (#A4544), hydrocortisone (#H0888), (FITC)-labeled dextran of 4 kDa (#FD-4), Phalloidin-FITC (#P5282) and Hoechst were purchased from Sigma-Aldrich, The Netherlands. Nile blue acrylamide (NLB, #25395) was purchased from Polysciences, Inc., Germany, cellulose dialysis tubes with 6-8 kDa cutoff were obtained from Spectrum™ and ethanol 96 %vol was from AnalaR NORMAPUR®-VWR, The Netherlands. Endothelial basal medium 2 (EBM-2, #CC-3156) was bought from Lonza. Fetal bovine serum (FBS, #10500-064), HEPES (#15630106), chemically defined lipid concentrate (#11905-031) and 1× Hank's balanced salt solution (HBSS, #14025050) were obtained from Gibco, while basic fibroblast growth factor (#100-18D) was from Peprotech. Trypsin-EDTA (0.05%, #25300062) and penicillin–streptomycin (#15140122) were purchased from Thermo Fisher Scientific Inc. Rat tail collagen type-I was purchased from Enzo Life Sciences (#ALX-522-435, LOT 08071815 or LOT 04201734).

Nanogel synthesis

Nanogels were synthesized by precipitation polymerization as previously described with some adaptations to suit this study purposes.[27] Briefly, NIPMAM (Sigma-Aldrich #423548), Nile blue acrylamide (NLB, Polysciences #25395), BIS (Sigma-Aldrich #146072) and sodium dodecyl sulfate (SDS) were added to a 100 ml glass round-bottom flask and dissolved in 45 ml of filtered ddH_2O (0.2 μm Whatman filter), stirred and purged with N_2. The solution was placed in an oil bath at 70 °C and ammonium persulfate (APS, Sigma-Aldrich #A3679) dissolved in ddH_2O and purged with N_2 that was added after 30 min. Polymerization time was recorded after addition of APS. It should be noted that NLB is a polymerizable fluorescent monomer and copolymerizes with NIPMAM and BIS**.** Prior to use, NIPMAM 97% was purified by recrystallization from n-hexane and dried at reduced pressure using a rotary evaporator. Table 1 details the formulation conditions of the different nanogels used in this study. The cross-linking degree affects nanogel stiffness. The SDS concentration (Figure S1, Supplementary material) and polymerization time (Figure S2, Supplementary material) affect nanogel size and dispersity and were varied to obtain monodisperse nanogels with a mean diameter of 200 and 400 nm.

Table 1
Synthesis conditions for p(NIPMAM) nanogels with different cross-linking densities.

Nanogel	NIPMAM		BIS		SDS	NLB	APS	Polymerization time
	mg	mol %	mg	mol %	mmol l^{-1}	mg	mg	h
NG1.5	626	98.5	12	1.5	1.6	8	11	4
NG5	604	95	39	5	2.5	10	11	2.5
NG14	604	86	117	14	2.5	10	11	2.5
$NG5^{large}$	604	95	39	5	1.6	10	11	>6

All reactions were performed at 70 °C in an oil bath.

Nanogel dialysis was performed until free dye was no longer visible by naked eye, which means dialysis typically was performed for 12 days: 10 days in ethanol 96 %vol (AnalaR NORMAPUR®-VWR), in which Nile blue and Nile blue acrylamide are very soluble, followed by ≥2 days of dialysis in ddH_2O using a cellulose dialysis tube (6-8 kDa cutoff, Spectrum™). Typically, the dialysis medium was changed 2-3 times a day. In the UV–vis spectrum of the dialysate 6 h after the last solvent change no absorption peak was detectable, confirming the absence of free dye in the nanogel formulation. After dialysis, the nanogels were freeze-dried.

Nanogel characterization

Hydrodynamic diameter and PdI at 37 °C, zeta potential (ζ-potential) and temperature-dependent behavior were determined using a Zetasizer Nano ZS (Malvern Instruments). The nanogels show a thermoresponsive behavior shifting between swollen and collapsed states with volume phase transition temperature (VPTT) at 44 °C,[27] being swollen at 37 °C, i.e., at physiological body temperature, and collapsed at temperatures >44 °C. 20 μg ml^{-1} of nanogels in 1 mmol l^{-1} SDS in ddH_2O was used to obtain the thermoresponsive curves between 20 and 60 °C with 2 °C intervals and an equilibration time of 180 s. The swelling ratio reflects the nanogel cross-linking density and was determined by calculation of the ratio between the hydrodynamic diameter of the nanogel formulation at 50 °C and 20 °C. ζ-potential was determined in ddH_2O (Table S1) and complete cell culture

Table 2
p(NIPMAM) nanogel properties.

	Z-average at 37 °C (nm)	PdI	TEM size (mean ± SD) (nm)	Swelling ratio (d_{20}/d_{50})	ζ-potential at 37 °C (mV)[b]
NG1.5	170 ± 44	0.07	148 ± 18 (25)[a]	2.4 ± 0.1	−3.2 ± 0.8
NG5	230 ± 64	0.04	222 ± 56 (101)[a]	1.9 ± 0.1	−1.4 ± 0.3
NG14	175 ± 40	0.02	163 ± 56 (107)[a]	1.5 ± 0.02	−1.1 ± 0.3
$NG5^{large}$	423 ± 118	0.06	474 ± 121 (379)[a]	2.1 ± 0.08	−1.5 ± 0.8

[a] Number of particles measured from TEM images to estimate nanogel size.
[b] NGs ζ-potential was performed in EBM-2 medium with supplements at 37 °C with samples conductivity of 16.6 ± 0.7 mS cm^{-1}.

medium containing 5% (v/v) fetal bovine serum (FBS) after 2 h incubation at 37 °C to allow protein corona formation (Table 2).

TEM images were acquired on a transmission electron microscope and analyzed using Fiji.[28] At least 100 particles were measured to obtain the size range, except for 1.5 mol% BIS where 25 particles were measured due to sample limitation. Negative staining of nanogels drop-casted over carbon film coated copper grids was performed with 5 μl of 2% uranyl acetate. Samples were investigated with a Philips CM120 electron microscope coupled to a 4k CCD camera operated at 120 kV.

Brain endothelial cell culture

Human cerebral microvascular endothelial cell line (hCMEC/D3) cells were cultured in endothelial basal medium 2 (EBM-2; Lonza, #CC-3156) supplemented with 5% (v/v) FBS, 5 μg ml^{-1} ascorbic acid (Sigma-Aldrich #A4544), 1 ng ml^{-1} basic fibroblast growth factor (Peprotech, #100-18D), 1% (v/v) chemically defined lipid concentrate (Gibco #11905-031), 10 mmol l^{-1} HEPES (Gibco #15630106), 1.4 μmol l^{-1} hydrocortisone (Sigma # H0888) and 1% (v/v) penicillin–streptomycin in 25 cm^2 flasks coated with 150 μg ml^{-1} rat tail collagen type-I (Enzo Life Sciences, #ALX-522-435, LOT 08071815 or LOT 04201734). From a confluent flask with 4 to 6 × 10^5 cells per flask, split ratio was 1:10 with one medium change after 2 days and harvesting on the third day. Cells were grown at 37 °C in an incubator with 5% CO_2 atmosphere and used for experiments between passages 28 and 38.

Flow cytometry assessment of nanogel uptake in polarized brain endothelial cell monolayers

hCMEC/D3 cells were seeded in 24-well plates pre-coated with 150 μg ml^{-1} rat tail collagen type-I at a density of 1 × 10^5 cells per cm^2. Cells were grown for 5 days and medium was changed every other day. At the 5th day, medium was removed, and cells were washed once with 1× HBSS. 500 μl of 100 μg ml^{-1} nanogel in EBM-2 complete medium was added to each well and incubated for 15, 30 and 120 min. After incubation, medium containing nanogels was removed, cells were washed twice with 1× HBSS and 200 μl trypsin-EDTA was added per well and incubated for 5 min for cell detachment. 400 μl of EBM-2 complete medium was added to each well, cells were pipetted vigorously up and down at least 10 times and samples were collected. Wells were washed once with 200-400 μl of 1× HBSS to collect remaining cells. Samples were centrifuged (500 ×*g*, 5 min, 4 °C), the supernatant was discarded, and the cells were resuspended in 400 μl of ice-cold 1× PBS supplemented with 2% (v/v) FBS and 5 mmol l^{-1} EDTA (PFE buffer). For experiments at 4 °C, the cell monolayer was incubated at 4 °C for 30 min and ice-cold 1× HBSS was used to wash the cells prior to ice-cold nanogel incubation for 2 h at 4 °C. Nanogels were removed and cells washed with ice-cold 1× HBSS two times, followed by trypsinization. Fluorescence in cells was measured with a CytoFlex S Flow Cytometer (Beckman Coulter) using the APC channel (670/30 band-pass filter) and laser excitation 640 nm. Data were analyzed using FlowJo V10 software (Tree Star, Inc.) and Origin. Because the different Nile blue-labeled nanogels do not have the same fluorescence intensity, the geometric mean fluorescence values were corrected according to the fluorescence of each nanogel at 656 nm ($\lambda_{excitation}$ = 633 nm) at 100 μg ml^{-1} in EBM-2 complete medium (Figure S3, Supplementary material) in order to compare the cellular uptake of the different nanogels.[29]

Transcytosis assay

Transcytosis assays were performed using a filter-free blood–brain barrier model previously described in detail by our group.[30] In short, collagen gels were prepared from a 5 mg ml^{-1} rat tail collagen type-I sterile solution in 0.02 N acetic acid that was neutralized by 1 mol l^{-1} NaOH, made isotonic from 10× phosphate-buffered saline (PBS) and diluted to 2 mg ml^{-1} with sterilized ddH_2O and final buffer composition of 1× PBS. hCMEC/D3 cells were grown over the collagen gels for 5 days at initial seeding density of 1 × 10^5 cells per cm^2; the medium was changed every other day and cells were washed with HBSS at day 2 and 5. After 5 days, the cell monolayer reached confluency and nanogel transcytosis was assessed as well as monolayer permeability. At 100 μg ml^{-1} in complete EBM-2 medium, 500 μl of NG1.5, NG5, $NG5^{large}$, and NG15 were incubated for 2, 4 or 16 h after washing the cell layer once with 1× HBSS. One hour before the end of the incubation period, 55 μl of 5 mg ml^{-1} fluorescein isothiocyanate (FITC)-labeled dextran of 4 kDa (Sigma-Aldrich #FD-4) was added to the apical compartment to evaluate paracellular permeability. Subsequently, the apical medium was aspirated, and hCMEC/D3 cells were separated from the basal medium by means of collagenase A treatment, as previously described.[30] Fluorescence was measured in the apical, cell, and basal fractions (excitation at 633 nm and emission at 680 nm). Cell monolayers that were treated without nanogel served as a control for the influence of collagenase A on nanogel fluorescence. The percentage of nanogels associated to a compartment – apical, cell or basolateral – was calculated with the formula below.

$$\%\text{nanogels} = (\text{compartment fluorescence})/(\text{total fluorescence}) \times 100 \quad [1]$$

Apparent permeability (P_{app}) was calculated using the following equation

$$P_{app} = (\Delta Q/\Delta t) \times (1/AC_0) \quad [2]$$

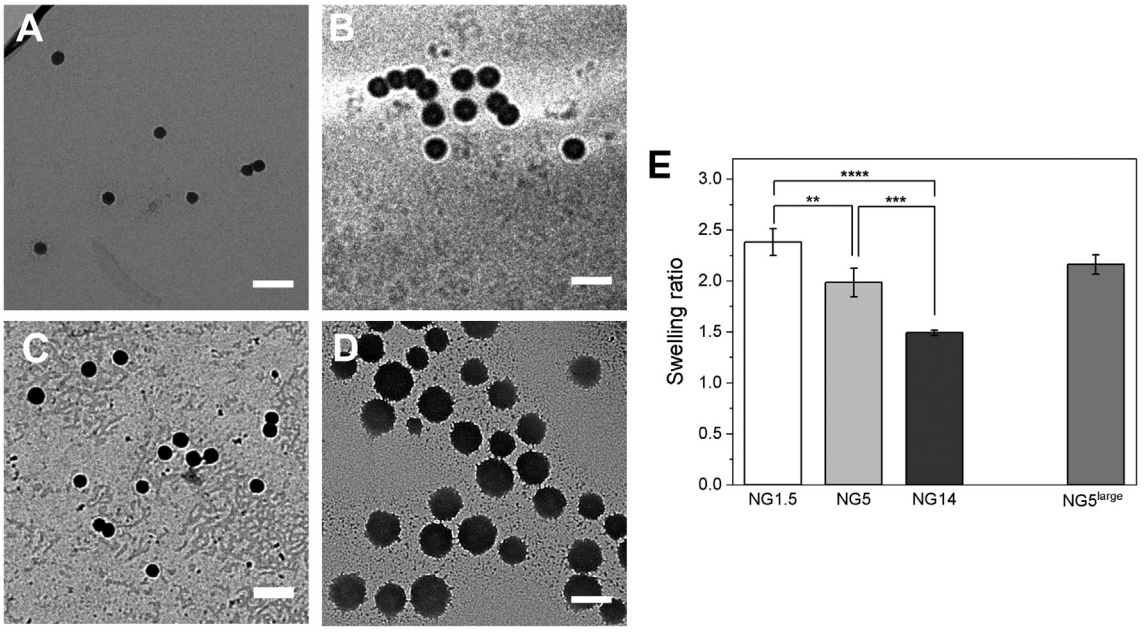

Figure 1. p(NIPMAM) nanogel characterization**.** P(NIPMAM) nanogel images obtained by negative staining followed by transmission electron microscopy. **(A)** 1.5 mol% BIS (NG1.5), **(B)** 5 mol% BIS (NG5), **(C)** 14 mol% BIS (NG14) and **(D)** 5 mol% BIS (NG5^{large}). **(E)** Swelling ratio of NG1.5, NG5, NG14 and NG5^{large}. Bars: 500 nm. Represented values are mean ± SD of three experiments with at least 40,000 events. Data were analyzed using ANOVA and Tukey's post-hoc test and significant differences are indicated by * for P value < 0.05, ** for P value < 0.01, *** for P value < 0.005 and **** for P value < 0.0005.

where $\Delta Q/\Delta t$ represents the rate of permeation of dextran (μg min^{-1}), A is the surface area (cm^2), and C_0 is the initial concentration of FITC-dextran (μg ml^{-1}) added to the apical side. FITC-dextran fluorescence was recorded at λ_{ex} = 485 nm and λ_{em} = 520 nm. Apparent permeability was verified for all samples and assays. The fluorescence was measured using Synergy H1 Hybrid plate reader (BioTek Instruments Inc.)

To determine the extent by which internalized nanogels are exocytosed, the ratio of NG fluorescence associated with the basolateral compartment and within the cells was calculated, while the ratio for NG1.5 was set as 1.

Confocal microscopy of nanogels in polarized brain endothelial cell monolayers

Collagen gels were prepared on glass slides using polydimethylsiloxane (PDMS) gel as a mold (Supplementary material). hCMEC/D3 cells were seeded at an initial density of 1 × 10^5 per cm^2 and grown for 5 days in complete EBM-2 medium. Medium was changed every day. After 5 days, medium was removed and the monolayer was washed once with 1× HBSS, followed by incubation with 50 μg of nanogel in 500 μl of complete EBM-2 medium for 2 h. 30 min before the end of the incubation period, Hoechst was added to the cells at a final concentration of 2 μg ml^{-1} as a guide for sample focusing for examination by confocal microscopy. Apical medium containing nanogels and Hoechst was removed and the cell monolayer was washed twice with 1× HBSS before fixation. Cells were incubated with 3.7% paraformaldehyde (PFA) in 1× PBS for 15 min, followed by 3 washes with 1× PBS and incubation with 0.2% (v/v) of Triton X-100 in PBS for 10 min. Then, the monolayer was washed with 1× PBS three times for 15 min under mild agitation. Cells were incubated with Phalloidin-FITC (Sigma-Aldrich #P5282) at 1:100 dilution for 90 min protected from light. Washing was performed three times, samples were mounted with PBS:glycerol (50:50) and a cover slip was carefully placed over the samples. Images were collected using a Leica TSC SP2 confocal microscope (63× immersion oil objective) and analyzed with Fiji software.[28] Z slice images were collected sequentially using two or three channels and excitation lasers 488 (ArKr) and 633 nm (HeNe). Ninety stacks were collected for each image, each image being an average of two frames composed of 512 × 512 pixels.

Results

Nanogel characterization

P(NIPMAM) nanogels of different stiffnesses were prepared by tuning their cross-linking densities and reactant contents. Nanogels of ~200 nm diameter were prepared with 1.5, 5, and 14 mol% BIS cross-linker, and nanogels of ~400 nm were prepared with 5 mol% BIS cross-linker. The size of the nanogels was determined by dynamic light scattering and confirmed by TEM (Table 2 and Figure 1, *A-D*). All nanogels showed a slightly negative ζ-potential when dispersed in cell culture medium (Table 2). Nanogels with a similar size and different cross-linking densities showed the highest swelling ratio for the nanogel with the lower amount of cross-linker (Table 2 and Figure 1, *E*). Moreover, the swelling ratio was significantly different between the nanogels with different cross-linking densities (NG1.5, NG5, NG14), but not between nanogels with similar cross-linking density (NG5 and NG5^{large}) (Table 2 and Figure 1, *E*). Nanogels with different sizes and the same cross-

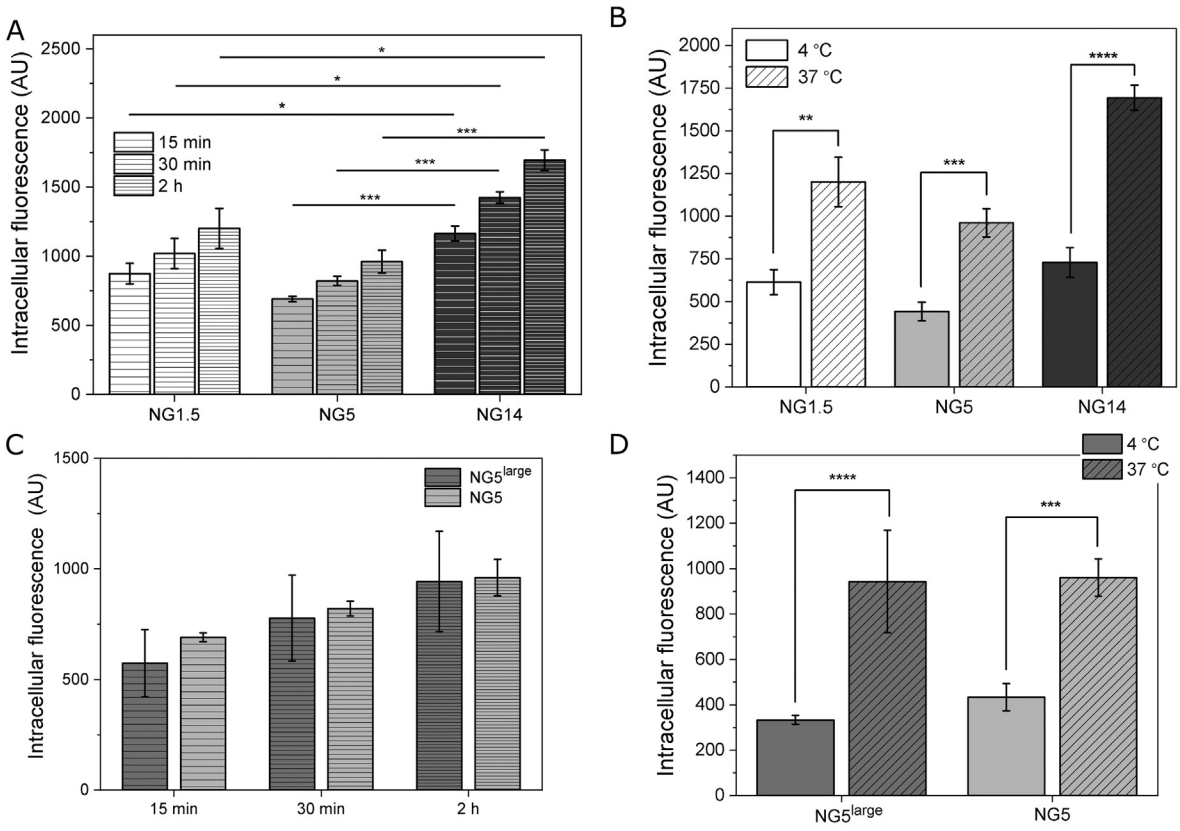

Figure 2. Effect of NG size and stiffness on NG uptake by hCMEC/D3 cell monolayers. hCMEC/D3 cell monolayers were incubated with Nile blue-labeled NG1.5, NG5, and NG14 at **(A)** 37 °C for 15, 30 and 120 min and **(B)** 4 °C and 37 °C for 2 h, after which intracellular fluorescence was determined by flow cytometry. hCMEC/D3 cell monolayers were incubated with Nile blue-labeled NG5, and NG5^{large} at **(C)** 37 °C for 15, 30 and 120 min and **(D)** 4 °C and 37 °C for 2 h, after which intracellular fluorescence was measured by flow cytometry. The cellular fluorescence intensities were corrected by dividing the mean fluorescence intensity of the cells by the fluorescence intensity of the NG stock dispersions (100 μg ml^{-1}). Represented values are mean ± SD of three experiments with at least 40,000 events. Data were analyzed using ANOVA and Tukey's post-hoc test **(A)**, and two-sample *t* test **(B, C, D)** and significant differences are indicated by * for *P* value < 0.05, ** for *P* value < 0.01, *** for *P* value < 0.005 and **** for *P* value < 0.0005.

linking density showed a similar swelling ratio (Table 2 and Figure 1, *E*).

Overall, the p(NIPMAM) nanogel thermoresponsive behavior revealed an inverse correlation between cross-linking density and swelling ratio, which is in accordance with literature, i.e., micro/nanogels with higher cross-linking density show a lower swelling ratio, which is indicative for an increase in stiffness.[27,31]. p(NIPMAM) microgels with similar cross-linking densities and swelling ratios displayed in our earlier work stiffnesses of 21 ± 8, 117 ± 20, and 346 ± 125 kPa, for 1.5, 5 and 15 mol% BIS, respectively, as were determined in previous work.[27] These results confirm that an increase in cross-linking density results in an increase in stiffness (Table 2). NGs with the same cross-linking density but different sizes showed the same swelling ratio and hence similar stiffness (Table 2; compare NG5^{large} (425 nm, 5 mol % BIS) and NG5 (230 nm, 5 mol% BIS)), indicating that NG stiffness is not size-dependent.

High nanogel stiffness favors uptake by polarized brain endothelial cell monolayers

Previous studies have indicated that stiffer particles generally present higher internalization levels in eukaryotic cells, including endothelial cells.[16,32] This phenomenon has been attributed to an easier wrapping of the plasma membrane of cells around stiff particles.[33] Here, the uptake of nanogels with varying stiffness, i.e., NG1.5, NG5, and NG14, was measured in polarized hCMEC/D3 cell monolayers. Fluorescently labeled nanogels were incubated with hCMEC/D3 cell monolayers for 15, 30, and 120 min at 37 °C. Figure 2, *A* shows that the uptake of NG1.5 and NG5 by hCMEC/D3 cells was not significantly different, although NG5 showed a tendency of lower internalization levels when compared to NG1.5. Nevertheless, the uptake of NG14 nanogels was significantly higher than that of NG1.5 and NG5. Specifically, NG14 showed 1.4 ± 0.2 and 1.8 ± 0.2 times higher cellular uptake than NG1.5 and NG5, respectively. In addition, the effect of nanogel size on uptake by hCMEC/D3 cell monolayers was investigated. To this end, two NG formulations with the same cross-linking density but different sizes, i.e., NG5 and NG5^{large}, were incubated with hCMEC/D3 cell monolayers for 15, 30, and 120 min (37 °C). Both types of NGs were internalized by hCMEC/D3 cells to a similar extent (Figure 2, *C*), indicating that NGs with a size of ~400 nm are internalized as efficiently as NGs of ~200 nm. Additionally, we assessed the cellular uptake of the nanogels at 4 °C, i.e., a temperature at which energy-dependent processes, including endocytosis, are inhibited. At 4 °C the uptake of nanogels by hCMEC/D3 cells was strongly

inhibited (Figure 2, *B*), indicating that nanogel uptake occurs via an active process.

To determine the intracellular distribution of the NGs in hCMEC/D3 cells, cells were incubated with fluorescently labeled NGs and investigated by confocal microscopy. Figure 3, *A* (and quantification in Figure 3, *B*) shows that virtually all cells in the cell monolayer contain NGs, which tend to accumulate at the perinuclear region. Furthermore, the cellular distribution after incubation at 37 °C was similar for all 4 NGs, where a dotted fluorescence pattern with nuclear exclusion rather than a diffuse fluorescence pattern was observed, suggesting a vesicular localization.[34] Of note, because of the different fluorescence intensities of the different NG formulations (see Figure S3, Supplementary material) a comparison of the uptake levels of the different NGs by direct visual inspection of the fluorescence images was not possible.

Low nanogel stiffness favors transcytosis across polarized brain endothelial cell monolayers

Next, the effect of NG stiffness on NG transport across an *in vitro* BBB model was investigated. To this end, 50 μg of Nile blue-labeled NG1.5, NG5, NG5^{large}, and NG14 was incubated at 100 μg ml^{-1} for 2, 4 and 16 h with the filter-free BBB model, after which the fluorescence in the apical, cell, and basal compartments was quantified. After 2 h incubation, the softer NG1.5 and NG5 particles showed an enhanced accumulation of 7.5 ± 0.9% and 6.7 ± 0.6%, respectively at the basal side of the cell monolayer compared to an accumulation of 5.2 ± 0.4% for the stiffest NG14 nanogel (Figure 4, *A*). Longer incubation periods resulted in a modest increase in basal accumulation of the NGs with again highest basal accumulation for NG1.5 and NG5 (Figure 4, *B* and *C*). NG5^{large} and NG5 exhibited a similar transcytotic capacity (Figure 4, *A-E*). To exclude possible paracellular transport of NGs due to a compromised BBB, the permeability (P_{app}) of the hCMEC/D3 cell monolayers for 4 kDa dextran, a marker for paracellular leakage, was evaluated during the final 60 min of incubation with the NGs. Incubation of cell monolayers with NGs did not induce an increase in the P_{app} for dextran compared to control cells, indicating that the barrier properties of the BBB model remained intact during incubation with NGs (Figure 4, *F*).

While the differences in basal accumulation of the different nanogels seem small, it should be noted that the soft NG1.5 and NG5 were less efficiently internalized by hCMEC/D3 cells, but showed a higher basal accumulation, compared to the stiff NG14. When we calculate the fraction of internalized nanogels that reached the basolateral compartment, it becomes evident that the softer NG1.5 and NG5 nanogels showed a two-fold higher secretion at the basal side of the hCMEC/D3 monolayer compared to the stiff NG14 nanogel (Figure 4, *D*).

To visualize the transcytosed fraction of NGs in the BBB model, hCMEC/D3 cell monolayers were grown on collagen gels in a PDMS mold (see Material and Methods), incubated for 2 h with fluorescently labeled NGs, and investigated by confocal microscopy. 3D image reconstruction of confocal Z-stacks, as presented in Figure 5, shows that NG1.5, NG5, as well as NG14 appeared at the basal side of the *in vitro* BBB and penetrated the collagen gel that supported the hCMEC/D3 cell monolayer. Specifically, the cytoskeletal component F-actin underlies the plasma membrane of the cells[35,36], and was stained (green) to indicate the apical and basal cell surfaces. NGs (red) were observed within the cells, i.e., in between the apical and basal surface. In addition, NGs were observed directly underneath the basal actin layer, and at locations further into the collagen gel, indicating NG exit from the cells.

Discussion

To investigate the influence of nanoparticle stiffness on nanoparticle transport across the blood–brain barrier, p(NIPMAM) nanogels with different cross-linking densities, i.e., 1.5 mol%, 5 mol%, and 14 mol% BIS were prepared. As expected, the cross-linking density of the NGs showed a positive correlation with their stiffness. Upon their incubation with an *in vitro* BBB model, composed of a polarized hCMEC/D3 cell monolayer grown on a collagen gel, the more densely cross-linked p(NIPMAM) nanogel (NG14) showed a significantly higher level of uptake by the polarized brain endothelial cells compared to NG1.5 and NG5, whereas the less densely cross-linked nanogels (NG1.5, NG5) demonstrated the highest transcytotic potential. These findings suggest that nanogel stiffness has opposing effects on nanogel uptake and transcytosis at the BBB. Simulations studies indicate that soft particles must overcome a high-energy barrier to induce their enwrapping by the plasma membrane of cells. This is due to the fact that soft particles induce low membrane bending, which is caused by their spreading over the cell surface due to particle deformation.[24,33,37] Moreover, using coarse-grained molecular dynamics simulations Shen et al showed that the difference in wrapping efficiency of soft and rigid particles scales with particle size.[38] Because soft particles show higher deformation and induce less membrane bending, the energy barrier they need to overcome in order to become fully enwrapped is higher and, consequently, more receptors need to be recruited to provide the required driving force for their uptake. Consequently, the uptake of large particles is less influenced by particle stiffness than the uptake of small particles. With that in mind, we could explain the lack of significant variation in uptake between NG1.5 and NG5 (Figure 1, *A*) as an insufficient variation in particle stiffness ($\Delta E_{NG5\text{-}NG1.5}$ = 96 kPa) for particles in the 150-250 nm size range, and suggest that there is a rather sharp response toward NG stiffness.

In addition, stiffer nanoparticles (>200 kPa) were shown to favor clathrin-dependent endocytosis, while softer particles were taken up via macropinocytosis or a combination of endocytic pathways.[21,40] Therefore, it could be speculated that nanogels of different stiffnesses are internalized via different endocytic pathways that exhibit different uptake (and transcytosis) efficiencies. Furthermore, nanoparticle stiffness has been shown to influence protein corona formation, which will also influence the interaction of the nanogels with cells. Although protein corona formation on nanoparticles is extensively being investigated,[45] there are just few studies describing the protein corona of nanogels.[25,26,46–48] These studies showed that protein adhesion to nanogels is low compared to adhesion to nanoparticles, while nanogel hydrophobicity promotes protein

A

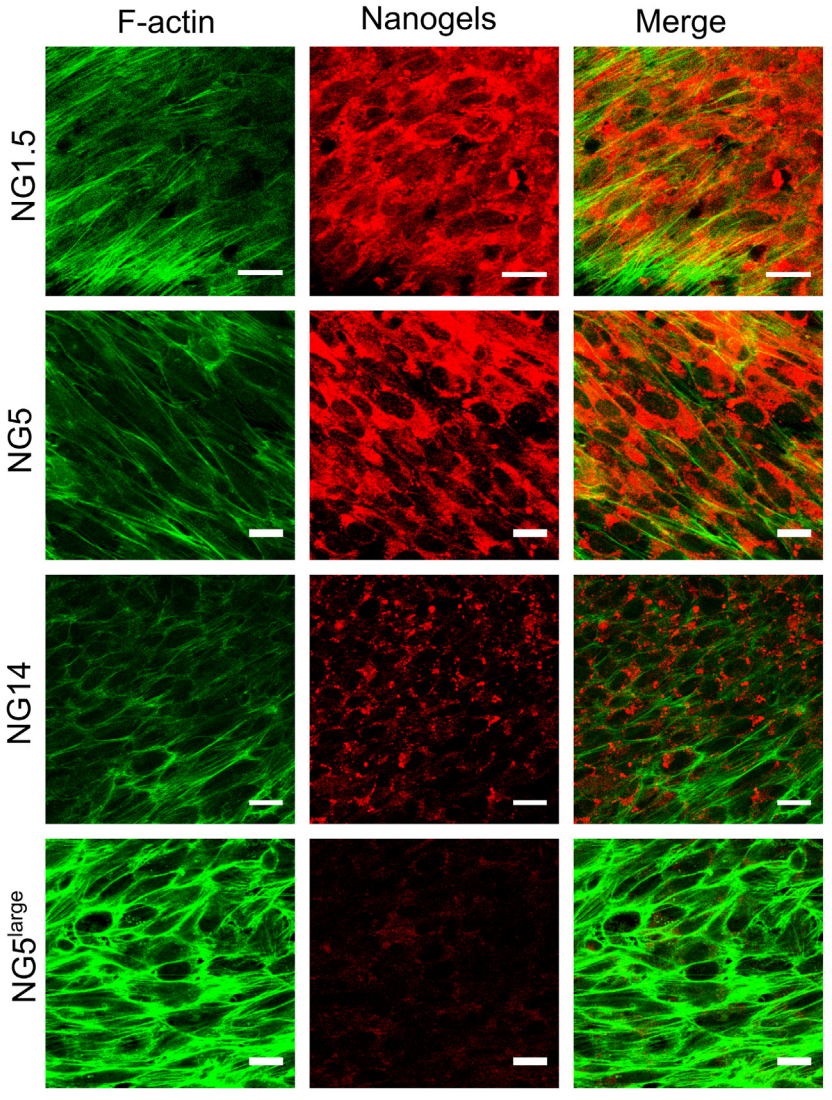

B

Nanogel	% positive cells (APC+)		
	15 min, 37°C	30 min, 37°C	2 h, 37°C
NG1.5	99.93 ± 0.05	100	99.97 ± 0.05
NG5	99.8 ± 0.2	99.9 ± 0.1	99.93 ± 0.05
NG14	99.7 ± 0.2	99.77 ± 0.09	99.87 ± 0.09
NG5^{large}	98.8 ± 0.4	99.5 ± 0.2	99.7 ± 0.2

Figure 3. **(A)** Cellular distribution of NG1.5, NG5, NG14 and NG5^{large} in hCMEC/D3 cell monolayers. hCMEC/D3 monolayers were incubated with NG1.5, NG5, NG14 and NG5^{large} for 2 h at 37 °C, followed by fixation, F-actin staining, and examination by fluorescence microscopy. Scale bars are 20 μm. Images were acquired using the same microscopy settings. **(B)** Percentage of Nile blue-positive (APC+) hCMEC/D3 cells following 15 min, 30 min, and 2 h incubation with Nile blue-labeled nanogels with different cross-linking densities and sizes, as obtained by flow cytometry.

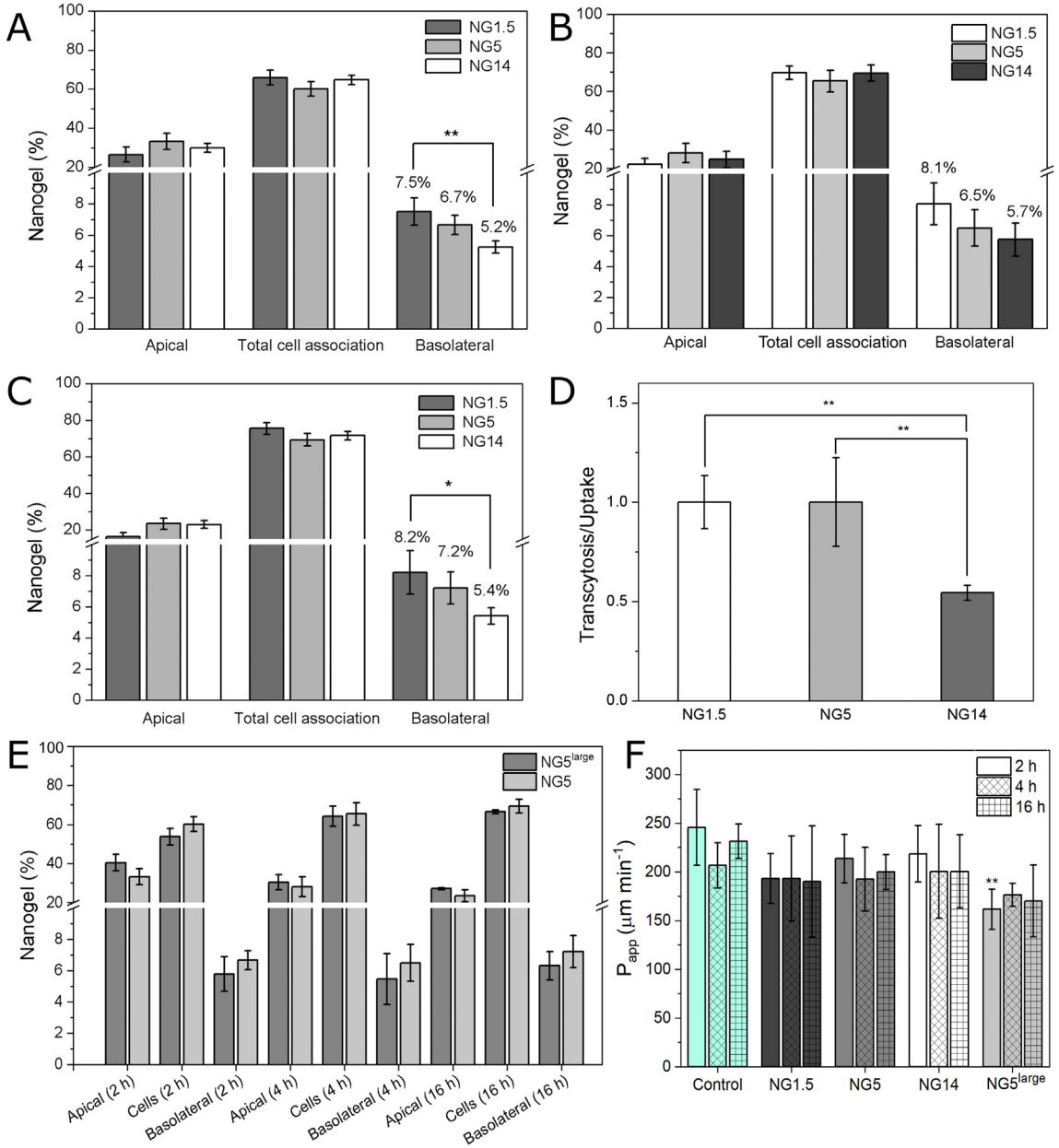

Figure 4. Effect of NG size and stiffness on NG transport across an *in vitro* filter-free BBB model. hCMEC/D3 cell monolayers were incubated with Nile blue-labeled NG1.5, NG5, and NG14 at 37 °C for **(A)** 2, **(B)** 4, and **(C)** 16 h, after which fluorescence in the apical, cell, and basal fractions was determined by fluorescence spectroscopy. **(D)** Fraction of internalized nanogels that underwent exocytosis expressed as the ratio of NG fluorescence in the basal compartment in the transcytosis assay and in the cell fraction in the uptake assay, after 2 h incubation with NG1.5, NG5, and NG14. The ratio for NG1.5 was set as 1. **(E)** Transcytosis levels for NG5 and NG5^{large} after 2, 4 and 16 h incubation. **(F)** Apparent permeability (P_{app}) of FITC-dextran (MW 4 kDa) in hCMEC/D3 cell monolayers incubated with NG1.5, NG5, NG14 and NG5^{large} for 2, 4 and 16 h. Control is hCMEC/D3 cell monolayer incubated without nanogel. Values are represented as mean ± SD of four independent experiments and each experiment was performed in duplicate. Data were analyzed using ANOVA and Tukey's post-hoc test and significant differences are indicated by * for P value < 0.05, ** for P value < 0.01.

adhesion. Altogether, because of both direct and indirect effects of NG stiffness on their interaction with cells, it may not be surprising that NG uptake does not show a linear relationship with stiffness.

Taken together, our data show that increased levels of p (NIPMAM) NG uptake by hCMEC/D3 brain endothelial cells do not necessarily lead to improved NG transport across the BBB, highlighting the importance of intracellular trafficking and exocytosis in determining transport efficiency of NGs across endothelial barriers. Similarly, Freese et al[40] demonstrated that elevated cell association of poly(2-hydroxypropylmethacrylamide) coated-gold nanoparticles did not result in their improved transport across the BBB, which was attributed to the confinement of the particles in intracellular vesicles. A negative correlation between ligand-receptor affinity and transcytosis has been observed for TfR antibodies.[13,41] Intermediate ligand-receptor

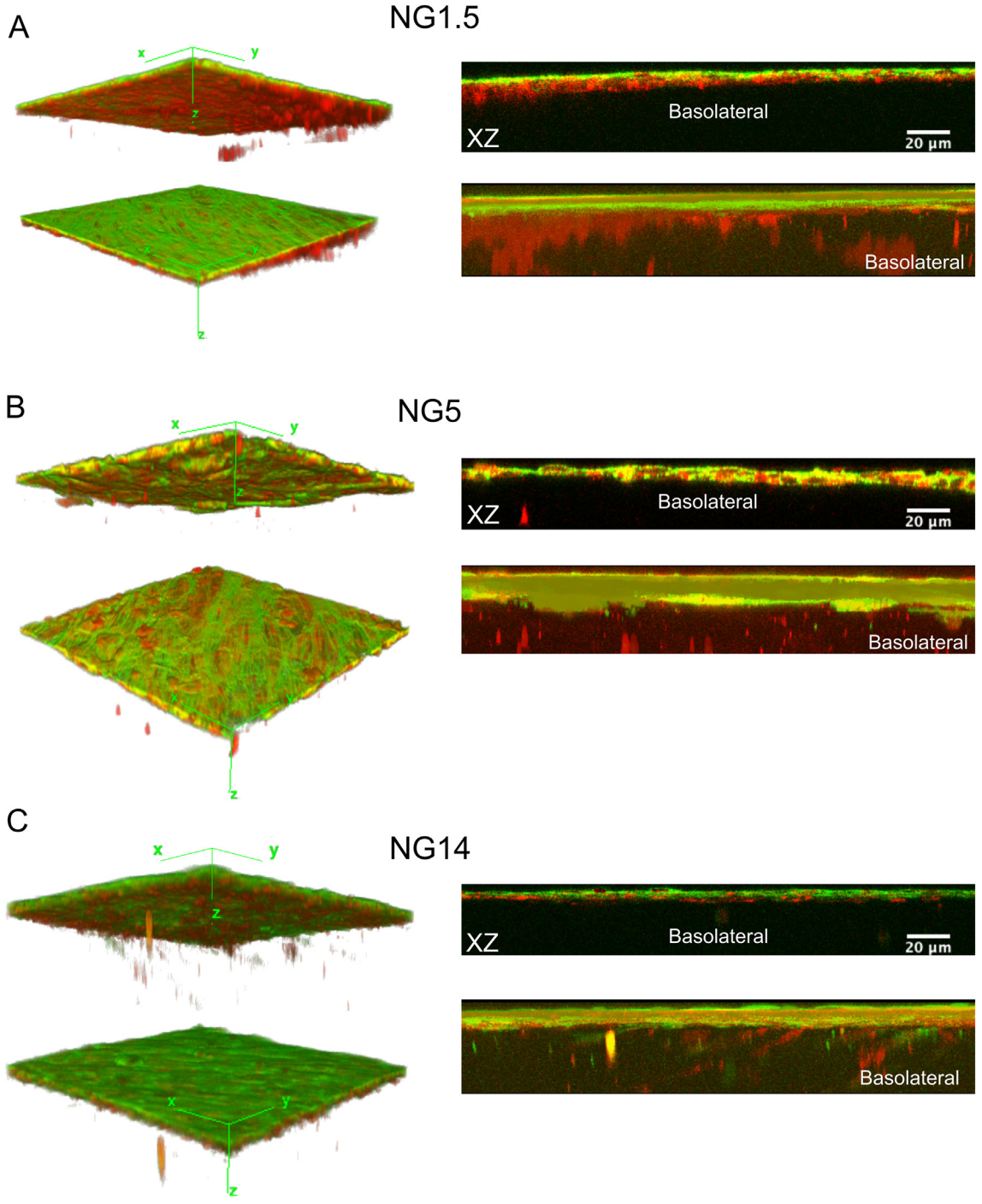

Figure 5. Basolateral accumulation of NG1.5, NG5, and NG14 at an *in vitro* filter-free BBB model. hCMEC/D3 cell monolayers were incubated with NG1.5, NG5, and NG14 for 2 h at 37 °C, followed by fixation, F-actin staining, and examination by confocal fluorescence microscopy. 3D image construction of Z-stacks (left) displays basolateral (top) and apical (bottom) views of cell monolayers incubated with **(A)** NG1.5, **(B)** NG5, and **(C)** NG14. XZ orthogonal views (right, top), and three-dimension projections (right, bottom). Images were acquired using the same microscopy settings. Red: nanogels; Green: F-actin.

affinity was shown to promote TfR antibody transcytosis, while high affinity was connected to delivery to lysosomes. A similar positive correlation between intermediate ligand-receptor affinity and transcytosis at the BBB has been reported for receptors at the BBB other than the transferrin receptor.[42,43] However, intermediate affinity of ligand-decorated nanoparticles to cells generally leads to lower uptake compared to nanoparticles with high affinity. Clark and Davis ingeniously obviated the need to use intermediate ligand-receptor affinity through the use of gold nanoparticles decorated with acid-cleavable ligands.[44] They demonstrated that gold nanoparticles functionalized with an acid-cleavable transferrin ligand reached the brain parenchyma at higher quantities compared to gold with non-cleavable transferrin (Tf). Following endocytosis of the gold nanoparticles, the separation between the

particle and Tf, as induced by a drop in endosomal pH, was held responsible for facilitating nanoparticle release at the basal side of the BBB. Whether decoration of soft nanogels with ligands improves their uptake without changing their transcytotic capacity remains to be investigated.

Since the process of transcytosis involves not only cellular uptake via endocytosis, but also intracellular vesicle trafficking and exocytosis, we hypothesize that low NG stiffness promotes intracellular trafficking and exocytosis. The enhanced intracellular trafficking and exocytosis of soft NGs compared to stiffer NGs can be a direct result of the low NG stiffness or an indirect result of an altered protein corona composition and/or routing via different endocytic/transcytotic pathways. Firstly, the lysosomal accumulation rate of nanoparticles was shown to be dependent on nanoparticle elasticity,[39] with hard nanoparticles exhibiting faster trafficking towards lysosomes, resulting in enhanced degradation. This means that soft NPs may have a better chance to escape from degradation and undergo transcytosis. Secondly, the altered protein corona composition of soft NGs compared to hard NGs may cause the NGs to take a different endocytic pathway that could be associated with increased transcytosis. Finally, reduced protein corona formation on soft nanogels may cause reduced affinity with the endosomal membrane, facilitating NP release at the basal side of the BBB. Further research is warranted to investigate these issues.

Overall, the data demonstrate that nanoparticle stiffness is an important parameter to be taken into account when designing nanoparticles that exploit transcytosis. Our finding that soft p (NIPMAM) nanogels are more efficiently transported across an *in vitro* BBB than their stiff counterparts could be exploited in the design of soft nanogels for drug delivery across the BBB, to improve current and future treatment of brain diseases.

Acknowledgments

LR was supported with an Abel Tasman Talent Program scholarship by the Graduate School of Medical Sciences (UMCG). This study was financed in part by the Coordenação de Aperfeiçoamento de Pessoal de Nível Superior-Brasil (CAPES), Finance Code 001. We thank Gwenda Vasse for help with flow cytometry measurements and PDMS mold preparation. We are grateful to Prof. dr. Anna Salvati for the use of the CytoFlex S Flow Cytometer (Beckman Coulter).

Appendix A. Supplementary data

Supplementary data to this article can be found online at https://doi.org/10.1016/j.nano.2021.102377.

References

1. Lin A, Sabnis A, Kona S, Nattama S, Patel H, Dong J-F, et al. Shear-regulated uptake of nanoparticles by endothelial cells and development of endothelial-targeting nanoparticles. *J Biomed Mater Res A* 2010;**93**:833-42, https://doi.org/10.1002/jbm.a.32592.
2. Ho YT, Kamm RD, Kah JCY. Influence of protein corona and caveolae-mediated endocytosis on nanoparticle uptake and transcytosis. *Nanoscale* 2018;**10**:12386-97, https://doi.org/10.1039/C8NR02393J.
3. Shilo M, Sharon A, Baranes K, Motiei M. Lellouche J-PM, Popovtzer R. The effect of nanoparticle size on the probability to cross the blood–brain barrier: an in-vitro endothelial cell model. *J Nanobiotechnol* 2015, https://doi.org/10.1186/s12951-015-0075-7 **13**:19.
4. Betzer O, Shilo M, Opochinsky R, Barnoy E, Motiei M, Okun E, et al. The effect of nanoparticle size on the ability to cross the blood–brain barrier: an in vivo study. *Nanomedicine* 2017;**12**:1533-46, https://doi.org/10.2217/nnm-2017-0022.
5. Georgieva JV, Kalicharan D, Couraud P-O, Romero IA, Weksler B, Hoekstra D, et al. Surface characteristics of nanoparticles determine their intracellular fate in and processing by human blood–brain barrier endothelial cells in vitro. *Mol Ther* 2011;**19**:318-25, https://doi.org/10.1038/mt.2010.236.
6. Sun W, Xie C, Wang H. Hu Y. Specific role of polysorbate 80 coating on the targeting of nanoparticles to the brain. *Biomaterials* 2004;**25**:3065-71, https://doi.org/10.1016/j.biomaterials.2003.09.087.
7. Stojanov K, Georgieva JV, Brinkhuis RP, van Hest JC, Rutjes FP, Dierckx RAJO, et al. In Vivo Biodistribution of prion- and GM1-targeted polymersomes following intravenous administration in mice. *Mol Pharm* 2012;**9**, https://doi.org/10.1021/mp200621v 1620-1627.
8. Lam FC, Morton SW, Wyckoff J, Vu Han T-L, Hwang MK, Maffa A, et al. Enhanced efficacy of combined temozolomide and bromodomain inhibitor therapy for gliomas using targeted nanoparticles. *Nat Commun* 2018;**9**, https://doi.org/10.1038/s41467-018-04315-4 1991.
9. Dal Magro R, Ornaghi F, Cambianica I, Beretta S, Re F, Musicanti C, et al. ApoE-modified solid lipid nanoparticles: a feasible strategy to cross the blood–brain barrier. *J Control Release* 2017;**249**:103-10, https://doi.org/10.1016/j.jconrel.2017.01.039.
10. Ohtsuki S, Terasaki T. Contribution of carrier-mediated transport systems to the blood–brain barrier as a supporting and protecting interface for the brain; importance for CNS drug discovery and development. *Pharm Res* 2007;**24**, https://doi.org/10.1007/s11095-007-9374-5 1745-1758.
11. Zensi A, Begley D, Pontikis C, Legros C, Mihoreanu L, Wagner S, et al. Albumin nanoparticles targeted with Apo E enter the CNS by transcytosis and are delivered to neurones. *J Control Release* 2009;**137**:78-86, https://doi.org/10.1016/j.jconrel.2009.03.002.
12. Neves AR, Queiroz JF, Lima SAC, Reis S. Apo E-functionalization of solid lipid nanoparticles enhances brain drug delivery: uptake mechanism and transport pathways. *Bioconjug Chem* 2017;**28**:995-1004, https://doi.org/10.1021/acs.bioconjchem.6b00705.
13. Yu YJ, Zhang Y, Kenrick M, Hoyte K, Luk W, Lu Y, et al. Boosting brain uptake of a therapeutic antibody by reducing its affinity for a transcytosis target. *Sci Transl Med* 2011;**3**:84ra44 LP-84ra44. doi:10.1126/scitranslmed.3002230.
14. Wiley DT, Webster P, Gale A, Davis ME. Transcytosis and brain uptake of transferrin-containing nanoparticles by tuning avidity to transferrin receptor. *Proc Natl Acad Sci* 2013;**110**:8662 LP - 8667. doi:10.1073/pnas.1307152110.
15. Hui Y, Wibowo D, Liu Y, Ran R, Wang H-F, Seth A, et al. Understanding the effects of nanocapsular mechanical property on passive and active tumor targeting. *ACS Nano* 2018;**12**, https://doi.org/10.1021/acsnano.8b00242 2846-2857.
16. Anselmo AC, Zhang M, Kumar S, Vogus DR, Menegatti S, Helgeson ME, et al. Elasticity of nanoparticles influences their blood circulation, phagocytosis, endocytosis, and targeting. *ACS Nano* 2015;**9**, https://doi.org/10.1021/acsnano.5b00147 3169-3177.
17. Yu M, Xu L, Tian F, Su Q, Zheng N, Yang Y, et al. Rapid transport of deformation-tuned nanoparticles across biological hydrogels and cellular barriers. *Nat Commun* 2018;**9**:2607, https://doi.org/10.1038/s41467-018-05061-3.
18. Zhao J, Lu H, Yao Y, Ganda S, Stenzel MH. Length vs. stiffness: which plays a dominant role in the cellular uptake of fructose-based rod-like micelles by breast cancer cells in 2D and 3D cell culture models? *J Mater Chem B* 2018;**6**, https://doi.org/10.1039/C8TB00706C 4223-4231.

19. Anselmo AC, Mitragotri S. Impact of particle elasticity on particle-based drug delivery systems. *Adv Drug Deliv Rev* 2017;**108**:51-67, https://doi.org/10.1016/j.addr.2016.01.007.
20. Hui Y, Yi X, Hou F, Wibowo D, Zhang F, Zhao D, et al. Role of nanoparticle mechanical properties in cancer drug delivery. *ACS Nano* 2019;**13**, https://doi.org/10.1021/acsnano.9b03924 7410-7424.
21. Guo P, Liu D, Subramanyam K, Wang B, Yang J, Huang J, et al. Nanoparticle elasticity directs tumor uptake. *Nat Commun* 2018;**9**:130, https://doi.org/10.1038/s41467-017-02588-9.
22. Wang S, Guo H, Li Y, Li X. Penetration of nanoparticles across a lipid bilayer: effects of particle stiffness and surface hydrophobicity. *Nanoscale* 2019;**11**, https://doi.org/10.1039/C8NR09381D 4025-4034.
23. Merkel TJ, Jones SW, Herlihy KP, Kersey FR, Shields AR, Napier M, et al. Using mechanobiological mimicry of red blood cells to extend circulation times of hydrogel microparticles. *Proc Natl Acad Sci* 2011;**108**:586 LP - 591. doi:10.1073/pnas.1010013108.
24. Yi X, Shi X, Gao H. Cellular uptake of elastic nanoparticles. *Phys Rev Lett* 2011;**107**98101, https://doi.org/10.1103/PhysRevLett.107.098101.
25. Obst K, Yealland G, Balzus B, Miceli E, Dimde M, Weise C, et al. Protein corona formation on colloidal polymeric nanoparticles and polymeric nanogels: impact on cellular uptake, toxicity, immunogenicity, and drug release properties. *Biomacromolecules* 2017;**18**, https://doi.org/10.1021/acs.biomac.7b00158 1762-1771.
26. Miceli E, Kuropka B, Rosenauer C, Osorio Blanco ER, Theune LE, Kar M, et al. Understanding the elusive protein corona of thermoresponsive nanogels. *Nanomedicine* 2018;**13**, https://doi.org/10.2217/nnm-2018-0217 2657-2668.
27. Keskin D, Mergel O, van der Mei HC, Busscher HJ, van Rijn P. Inhibiting bacterial adhesion by mechanically modulated microgel coatings. *Biomacromolecules* 2019;**20**:243-53, https://doi.org/10.1021/acs.biomac.8b01378.
28. Schindelin J, Arganda-Carreras I, Frise E, Kaynig V, Longair M, Pietzsch T, et al. Fiji: an open-source platform for biological-image analysis. *Nat Methods* 2012;**9**:676-82, https://doi.org/10.1038/nmeth.2019.
29. dos Santos T, Varela J, Lynch I, Salvati A, Dawson KA. Quantitative assessment of the comparative nanoparticle-uptake efficiency of a range of cell lines. *Small* 2011;**7**:3341-9, https://doi.org/10.1002/smll.201101076.
30. De Jong E, Williams DS, Abdelmohsen LKEA, Van Hest JCM, Zuhorn IS. A filter-free blood–brain barrier model to quantitatively study transendothelial delivery of nanoparticles by fluorescence spectroscopy. *J Control Release* 2018;**289**:14-22, https://doi.org/10.1016/J.JCONREL.2018.09.015.
31. Wedel B, Hertle Y, Wrede O, Bookhold J, Hellweg T. geSmart homopolymer microgels: influence of the monomer structure on the particle properties. *Polymers (Basel)* 2016;**8**, https://doi.org/10.3390/polym8040162.
32. Nowak M, Brown TD, Graham A, Helgeson ME, Mitragotri S. Size, shape, and flexibility influence nanoparticle transport across brain endothelium under flow. *Bioeng Transl Med* 2019;**n/a**:e10153. doi:10.1002/btm2.10153.
33. Yi X, Gao H. Cell membrane wrapping of a spherical thin elastic shell. *Soft Matter* 2015;**11**, https://doi.org/10.1039/C4SM02427C 1107-1115.
34. Pascual L, Cerqueira-Coutinho C, García-Fernández A, de Luis B, Bernardes ES, Albernaz MS, et al. MUC1 aptamer-capped mesoporous silica nanoparticles for controlled drug delivery and radio-imaging applications. *Nanomed Nanotechnol Biol Med* 2017;**13**:2495-505, https://doi.org/10.1016/j.nano.2017.08.006.
35. Weksler BB, Subileau EA, Perrière N, Charneau P, Holloway K, Leveque M, et al. Blood–brain barrier-specific properties of a human adult brain endothelial cell line. *FASEB J* 2005;**19**, https://doi.org/10.1096/fj.04-3458fje 1872-1874.
36. Latham SL, Chaponnier C, Dugina V, Couraud P-O, Grau GER, Combes V. Cooperation between β- and γ-cytoplasmic actins in the mechanical regulation of endothelial microparticle formation. *FASEB J* 2013;**27**:672-83, https://doi.org/10.1096/fj.12-216531.
37. Yi X, Gao H. Kinetics of receptor-mediated endocytosis of elastic nanoparticles. *Nanoscale* 2017;**9**:454-63, https://doi.org/10.1039/C6NR07179A.
38. Shen Z, Ye H, Yi X, Li Y. Membrane wrapping efficiency of elastic nanoparticles during endocytosis: size and shape matter. *ACS Nano* 2019;**13**:215-28, https://doi.org/10.1021/acsnano.8b05340.
39. Banquy X, Suarez F, Argaw A, Rabanel JM, Grutter P, Bouchard JF, et al. Effect of mechanical properties of hydrogel nanoparticles on macrophage cell uptake. *Soft Matter* 2009;**5**, https://doi.org/10.1039/b821583a 3984-3991.
40. Freese C, Unger RE, Deller RC, Gibson MI, Brochhausen C, Klok H-A, et al. Uptake of poly(2-hydroxypropylmethacrylamide)-coated gold nanoparticles in microvascular endothelial cells and transport across the blood–brain barrier. *Biomater Sci* 2013;**1**:824-33, https://doi.org/10.1039/C3BM60050E.
41. Haqqani AS, Thom G, Burrell M, Delaney CE, Brunette E, Baumann E, et al. Intracellular sorting and transcytosis of the rat transferrin receptor antibody OX26 across the blood–brain barrier in vitro is dependent on its binding affinity. *J Neurochem* 2018;**146**:735-52, https://doi.org/10.1111/jnc.14482.
42. Cooper PR, Ciambrone GJ, Kliwinski CM, Maze E, Johnson L, Li Q, et al. Efflux of monoclonal antibodies from rat brain by neonatal Fc receptor. *FcRn Brain Res* 2013;**1534**:13-21, https://doi.org/10.1016/j.brainres.2013.08.035.
43. Demeule M, Poirier J, Jodoin J, Bertrand Y, Desrosiers RR, Dagenais C, et al. High transcytosis of melanotransferrin (P97) across the blood–brain barrier. *J Neurochem* 2002;**83**:924-33, https://doi.org/10.1046/j.1471-4159.2002.01201.x.
44. Clark AJ, Davis ME. Increased brain uptake of targeted nanoparticles by adding an acid-cleavable linkage between transferrin and the nanoparticle core. *Proc Natl Acad Sci* 2015;**112**:12486 LP - 12491. doi:10.1073/pnas.1517048112.
45. Miceli E, Kar M, Calderón M. Interactions of organic nanoparticles with proteins in physiological conditions. *J Mater Chem B* 2017;**5**, https://doi.org/10.1039/C7TB00146K 4393-4405.
46. Lindman S, Lynch I, Thulin E, Nilsson H, Dawson KA, Linse S. Systematic investigation of the thermodynamics of HSA adsorption to N-iso-propylacrylamide/N-tert-butylacrylamide copolymer nanoparticles. Effects of particle size and hydrophobicity. *Nano Lett* 2007;**7**:914-20, https://doi.org/10.1021/nl062743+.
47. Pereira P, Pedrosa SS, Correia A, Lima CF, Olmedo MP, González-Fernández Á, et al. Biocompatibility of a self-assembled glycol chitosan nanogel. *Toxicol Vitr* 2015;**29**:638-646. doi:https://doi.org/10.1016/j.tiv.2014.11.004.
48. Bewersdorff T, Gruber A, Eravci M, Dumbani M, Klinger D, Haase A. Amphiphilic nanogels: influence of surface hydrophobicity on protein corona. *biocompatibility and cellular uptake Int J Nanomedicine* 2019;**14**, https://doi.org/10.2147/IJN.S215935 7861-7878.

Supporting Information:

LOW NANOGEL STIFFNESS FAVORS NANOGEL TRANSCYTOSIS ACROSS THE BLOOD-BRAIN BARRIER

Laís Ribovski[a,b], Edwin de Jong[a], Olga Mergel[a], Guangyue Zu[a], Damla Keskin[a], Patrick van Rijn[a], Inge S. Zuhorn[a,§]

[a] University of Groningen, University Medical Center Groningen, Department of Biomedical Engineering, Groningen, the Netherlands. A. Deusinglaan 1, 9713 AV Groningen, The Netherlands

[b] University of São Paulo, Physics Institute of São Carlos, Nanomedicine and Nanotoxicology Group, CP 369, 13560-970 São Carlos, SP, Brazil

[§] Corresponding author: Inge S. Zuhorn

E-mail address: i.zuhorn@umcg.nl

Nanogels size dependence of sodium dodecyl sulfate (SDS) concentration and polymerization time.

The presence of surfactants in the synthesis of nanogels affects size and monodispersity.[1,2] To obtain nanogels in the range of 200 and 400 nm, we study the polymerization time and SDS concentration effect on 5 mol% BIS nanogels. SDS concentration effect on nanogels size and dispersity was studied by preparing a solution containing 604 mg of NIPMAM, 39 mg of BIS (5 mol%), 10 mg of NLB and different concentrations of SDS from a 0.25 M SDS solution, at a final volume of 45 ml of ddH_2O in a round flask. This solution was left stirring under a N_2 flux for 30 min. After 30 min, the solution was placed in an oil bath at 70 °C still under stirring (400 rpm) for 30 min to reach temperature equilibration. In parallel, 11 mg of APS in 5 ml of ddH_2O was also under N_2 flux for 60 min. The initiator was added to the round flask containing NIPMAM, BIS, NLB and SDS using a syringe with a needle and the reaction has occurred for at least 6 h.

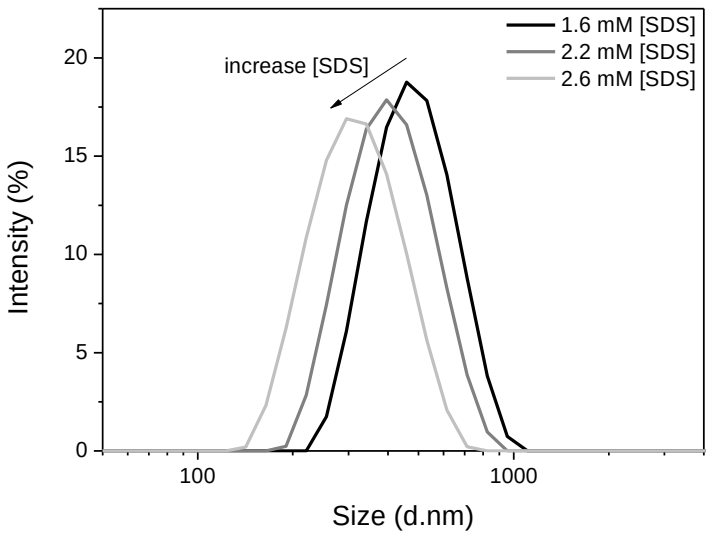

Figure S1 - Hydrodynamic diameter of p(NIPMAM) nanogels with 5 mol% BIS in ddH_2O synthesized in the presence of 1.6, 2.2 and 2.6 mM of SDS with polymerization time of at least 6 hours.

Figure S1 shows the size distribution of hydrodynamic diameter with different concentrations of SDS (1.6, 2.2 and 2.6 mM). It was observed that there is a limitation for SDS amount to produce monodisperse nanogels above 2.7 mM of SDS for 5 mol% BIS containing p(NIPMAM) nanogels even at concentrations below SDS critical micelle concentration of 8.2 mM in water.

To investigate nanogels size and dispersity as a function of polymerization time, the previously described synthesis conditions were employed with a fixed amount of SDS of 38 mg. Polymerization time is considered from the moment the initiator was added. To collect the samples at each time point, a syringe with a long needle was employed and 0.5 ml of sample was collected every 30 min. Between 90 and 240 min of reaction an increase in particle size is observed and, from 270 min of reaction there was no significant change of the size of the nanogels which relates to the consumption of the initiator, APS (Figure S2).

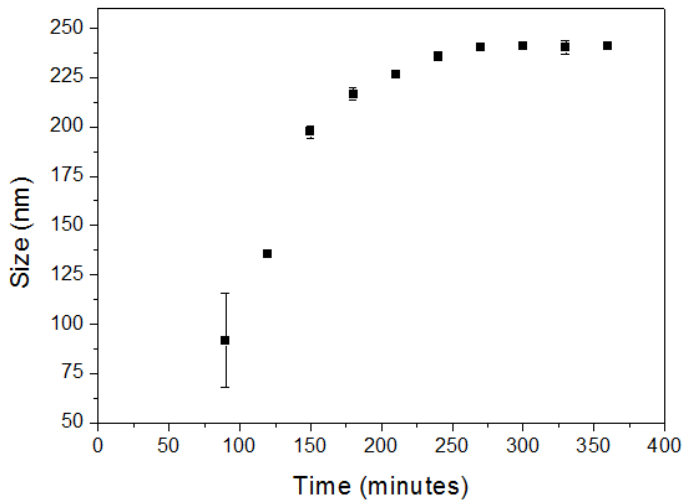

Figure S2 - P(NIPMAM) nanogels (5 mol% BIS) hydrodynamic diameter as function of polymerization time. Values represented are mean ± SD of 3 measurements from the same batch.

Nanogels zeta potential in ddH2O

ζ-potential was measured in ddH_2O besides cell culture complete medium (5% (v/v) FBS) and the result is displayed in Table S1.

Table S1 - Zeta potential of NGs of different cross-linking density and size in ddH_2O at room temperature (RT).

	ζ-potential at RT (mV)
NG1.5	-6.8 ± 3.1
NG5	-9.9 ± 6.5
NG14	-23.4 ± 7.9
$NG5^{large}$	-6.5 ± 5.5

Nanogels fluorescence and flow cytometry

The nanogels have different fluorescence intensities at same concentration. Figure S3a displays the spectra for each nanogels from 645 to 1000 nm with excitation at 633 nm.

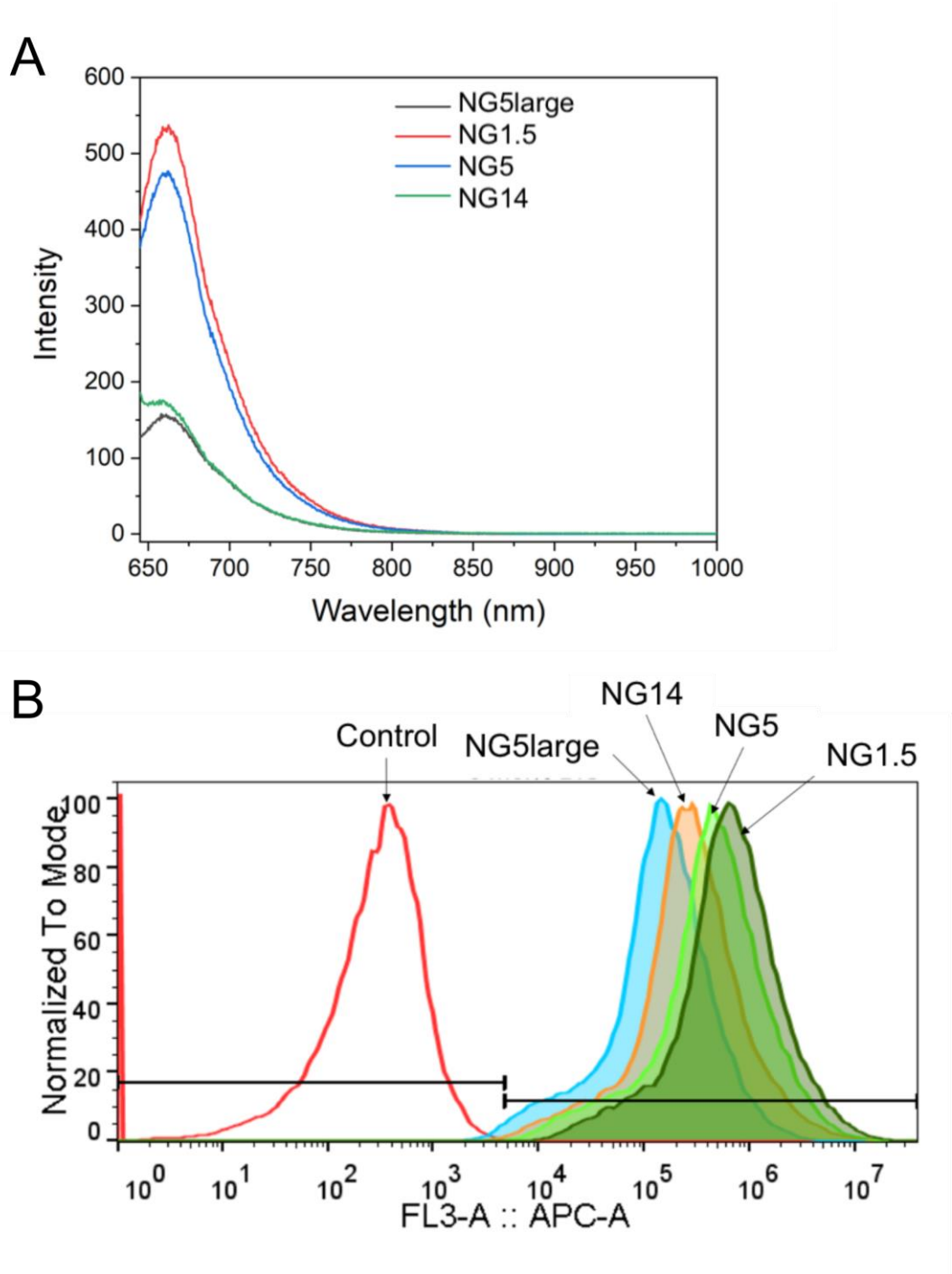

Figure S3 - A) Fluorescence spectra of nile blue in p(NIPMAM) nanogels dispersed in EMB-2 complete medium at 100 µg ml^{-1} with excitation at 633 nm and emission was recorded from 645 to 1000 nm, and B) flow cytometry histogram profiles of hCMEC/D3 cells after nanogels incubation for 2 hours at 37 ºC using the APC channel (670/30 band-pass filter) and laser excitation 640 nm.

Figure S3B show the histogram profile of each nanogel after 2 h incubation with hCMEC/D3 polarized cell layer highlighting the different fluorescence intensity between nanogels and in agreement with the spectra at Figure S3A.

PDMS mold preparation

Polydimethylsiloxane (PDMS) mold was prepared by mixing PDMS elastomer and silicone elastomer curing agent at mixing ratio 10:1 of curing agent to elastomer using the Sylgard^{TM} 184 Silicone Elastomer Kit. The mix was degassed and poured in a plastic plate and left curing overnight at 70ºC. PDMS gel was cut and holes were punched to be mold to the collagen gels. The pieces were placed over glass slides and plasma treated to bond PDMS to the glass (Figure S4A). To sterilize the pieces, they were placed at 180 °C for 4 h in closed glass containers further opened only under flow hood and transferred to 4 wells sterile plate where the collagen gel was placed inside the holes.

A

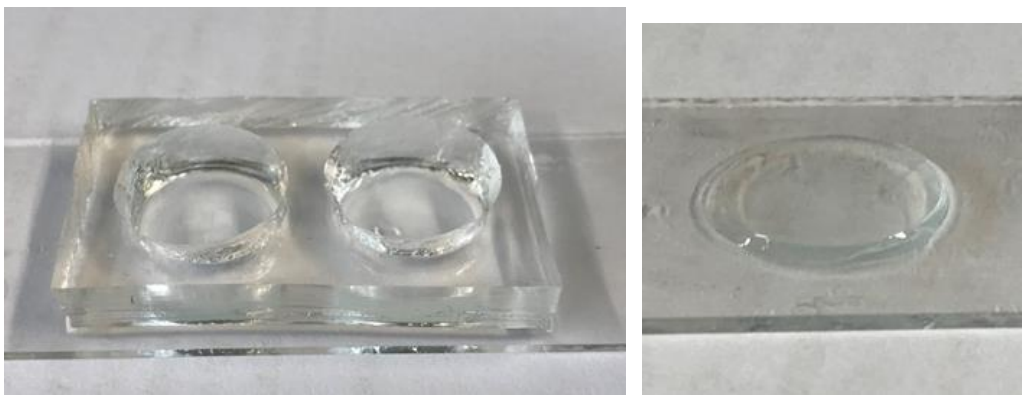

B

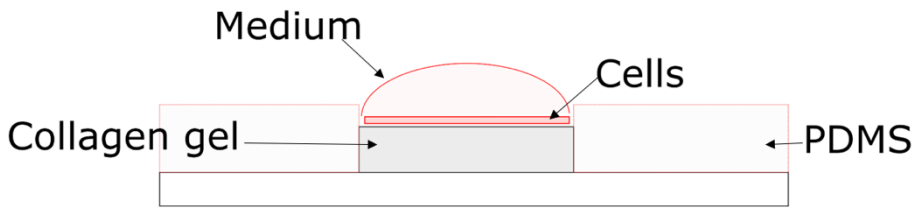

Figure S4 - A) PDMS mold after plasma treatment, B) hCMEC/D3 polarized layer on collagen gel after PDMS mold removal and C) schematic representation of PDMS mold containing collagen gel and hCMEC/D3 cell layer.

Figure S4B displays a collagen gel with a polarized cell layer after nanogel incubation and staining for microscopy followed by removal of PDMS mold and careful placement of a glass cover slip.

1. Wedel B, Brändel T, Bookhold J, Hellweg T. Role of Anionic Surfactants in the Synthesis of Smart Microgels Based on Different Acrylamides. *ACS Omega* 2017; **2**: 84–90. https://doi.org/10.1021/acsomega.6b00424.
2. von Nessen K, Karg M, Hellweg T. Thermoresponsive poly-(N-isopropylmethacrylamide) microgels: Tailoring particle size by interfacial tension control. *Polymer (Guildf)* 2013; **54**: 5499–5510. https://doi.org/https://doi.org/10.1016/j.polymer.2013.08.027.